# Supplemental material

## Invariant mass fit results

The results of the invariant mass fits for $\Xi_c^+$ and $\Lambda_c^+$ in $p$Pb and Pb$p$ data samples are shown in Fig. 5.

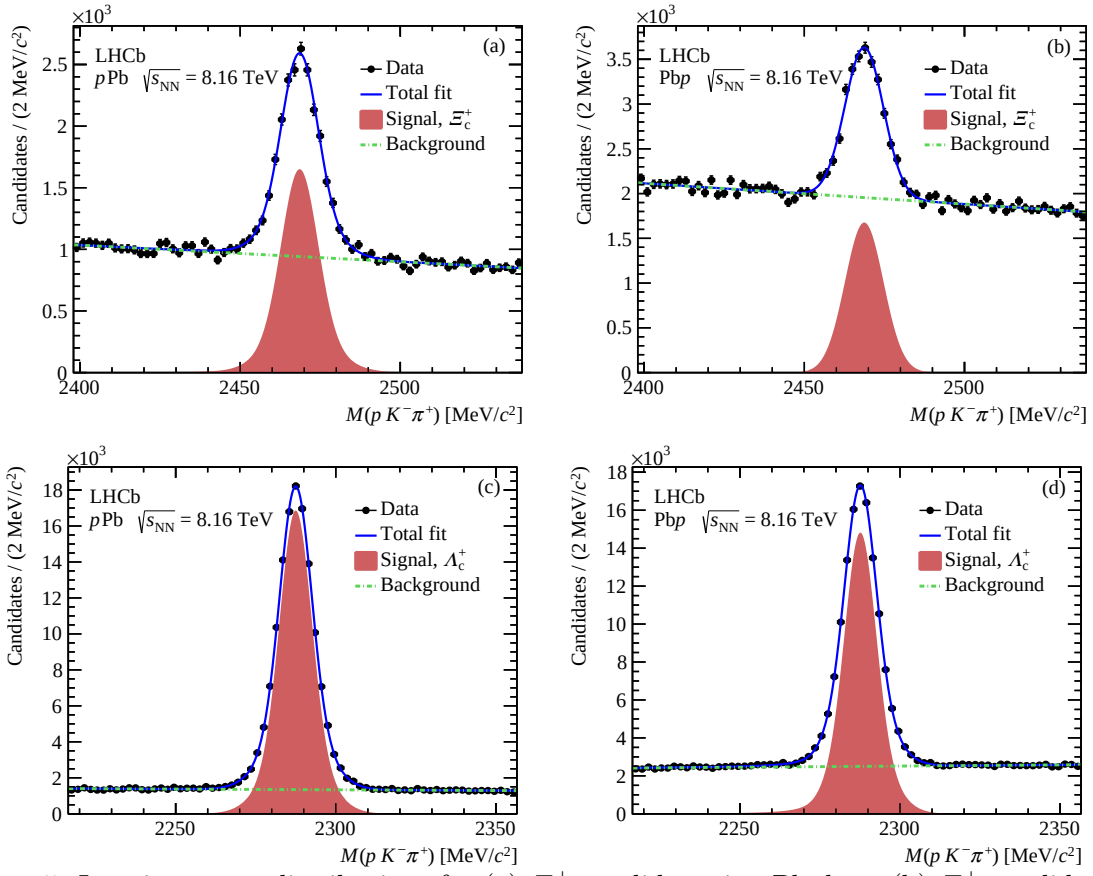


Figure 5: Invariant mass distributions for (a) $\Xi_c^+$ candidates in $p$Pb data, (b) $\Xi_c^+$ candidates in Pb$p$ data, (c) $\Lambda_c^+$ candidates in $p$Pb data, and (d) $\Lambda_c^+$ candidates in Pb$p$ data. The results of the fit are overlaid.

## Systematic uncertainties

Summaries of the systematic uncertainties in the $\Xi_c^+$ and $\Lambda_c^+$ cross-sections can be found in Tables 1, 2, and 3.

## Additional plots

The differential ratio of $\Xi_c^+$ to $\Lambda_c^+$ production multiplied by $\mathcal{B}(\Xi_c^+ \to pK^-\pi^+)$ is shown in Fig. 6 as a function of $p_{\rm T}$ and $y^*$.

Since LHCb has already measured the $D^0$ cross-section in $p$Pb collisions at $\sqrt{s_{\rm NN}} = 8.16\,\text{TeV}$ [42], we calculate the cross-section ratio $R_{\Xi_c^+/D^0} = \frac{\sigma(\Xi_c^+)}{\sigma(D^0)}$. Figure 7 shows $R_{\Xi_c^+/D^0}$ as a function of $p_{\rm T}$ (a) in both the forward and backward regions.

Table 1: Summary of systematic uncertainties on the $\Xi_c^+$ and $\Lambda_c^+$ cross-sections in $p_{\rm T}$ bins in the $p$Pb and Pb$p$ samples. The range of uncertainties correspond to the values obtained for different bins of $p_{\rm T}$.

| | $\Xi_c^+$ | | $\Lambda_c^+$ | |
|---|---|---|---|---|
| | $p$Pb | Pb$p$ | $p$Pb | Pb$p$ |
| Signal | 0.1 – 2.2% | 0.2 – 2.3% | – | – |
| Background | 1.3 – 5.7% | 0.5 – 18.0% | 0.1 – 1.0% | 0.1 – 0.8% |
| $\varepsilon_{\rm acc}$ | 0.1 – 0.2% | 0.1 – 0.3% | 0.1 – 0.2% | 0.1 – 0.2% |
| $\varepsilon_{\rm sel/rec}$ | 1.1 – 3.5% | 1.3 – 4.8% | 3.6 – 7.3% | 2.7 – 5.5% |
| $\varepsilon_{\rm PID}$ | 0.3 – 0.7% | 0.6 – 1.4% | 0.2 – 0.6% | 0.5 – 1.1% |
| $\varepsilon_{\rm trg/sel}$ | 0.4 – 0.5% | 0.4 – 0.5% | 0.1 – 0.6% | 0.4 – 0.8% |
| Total | 2.0 – 6.3% | 2.9 – 18.0% | 3.6 – 7.3% | 2.8 – 5.6% |

Table 2: Summary of systematic uncertainties on the $\Xi_c^+$ and $\Lambda_c^+$ cross-sections in $y^*$ bins in the $p$Pb and Pb$p$ samples. The range of uncertainties correspond to the values obtained for different bins of $y^*$.

| | $\Xi_c^+$ | | $\Lambda_c^+$ | |
|---|---|---|---|---|
| | $p$Pb | Pb$p$ | $p$Pb | Pb$p$ |
| Signal | 0.2 – 3.0% | 0.2 – 3.6% | 2.0 – 5.9% | – |
| Background | 0.1 – 5.7% | 1.7 – 27.4% | 0.1 – 4.6% | 0.7 – 17.7% |
| $\varepsilon_{\rm acc}$ | 0.1 – 0.4% | 0.1 – 0.8% | 0.1 – 0.3% | 0.1 – 0.5% |
| $\varepsilon_{\rm sel/rec}$ | 0.7 – 2.8% | 1.5 – 4.2% | 3.4 – 6.8% | 1.2 – 14.4% |
| $\varepsilon_{\rm PID}$ | 0.4 – 1.5% | 0.5 – 3.0% | 0.2 – 2.3% | 0.4 – 3.8% |
| $\varepsilon_{\rm trg/sel}$ | 0.4 – 0.5% | 0.4 – 0.6% | 0.4 – 0.5% | 0.4 – 1.2% |
| Total | 1.6 – 6.4% | 2.7 – 27.8% | 4.1 – 9.9% | 1.8 – 17.9% |

Table 3: Summary of systematic uncertainties correlated among bins on the $\Xi_c^+$ and $\Lambda_c^+$ cross-sections in the $p$Pb and Pb$p$ samples.

| | $p$Pb | Pb$p$ |
|---|---|---|
| Luminosity | 2.6% | 2.5% |
| Signal | 4.8% | 2.8–3.1% |
| Tracking | 5.5% | |
| $\mathcal{B}(\Xi_c^+ \to p^+K^-\pi^+)$ | 48.4% | |
| $\mathcal{B}(\Lambda_c^+ \to p^+K^-\pi^+)$ | 5.1% | |

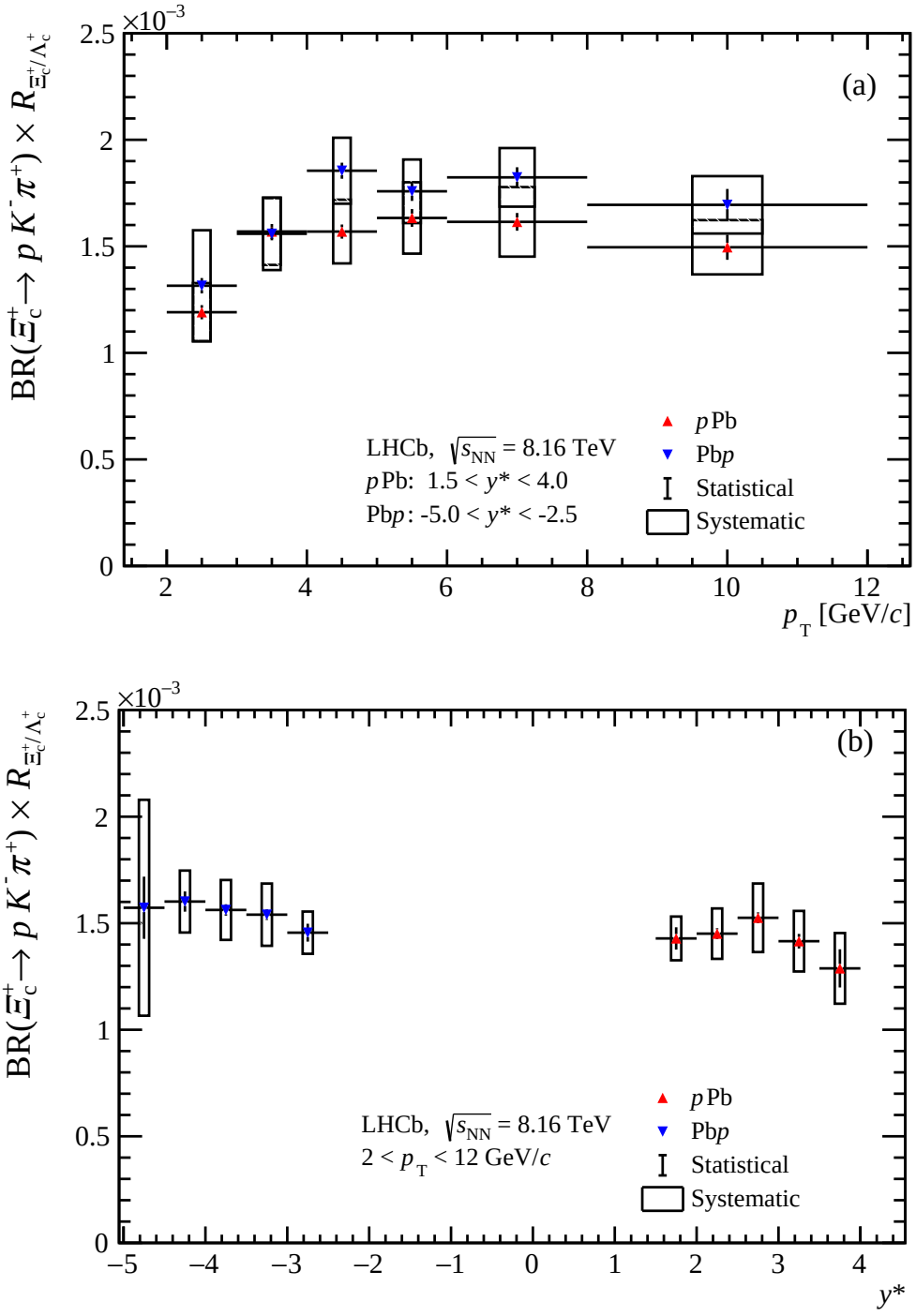


Figure 6: Production ratio of prompt $\Xi_c^+$ to $\Lambda_c^+$ baryons multiplied by $\mathcal{B}(\Xi_c^+ \to pK^-\pi^+)$ in $p$Pb (red triangles) and Pb$p$ (blue triangles) data samples as a function of (a) $p_{\rm T}$ and (b) $y^*$. The error bars represent the statistical uncertainties while the squares indicate the systematic uncertainty.

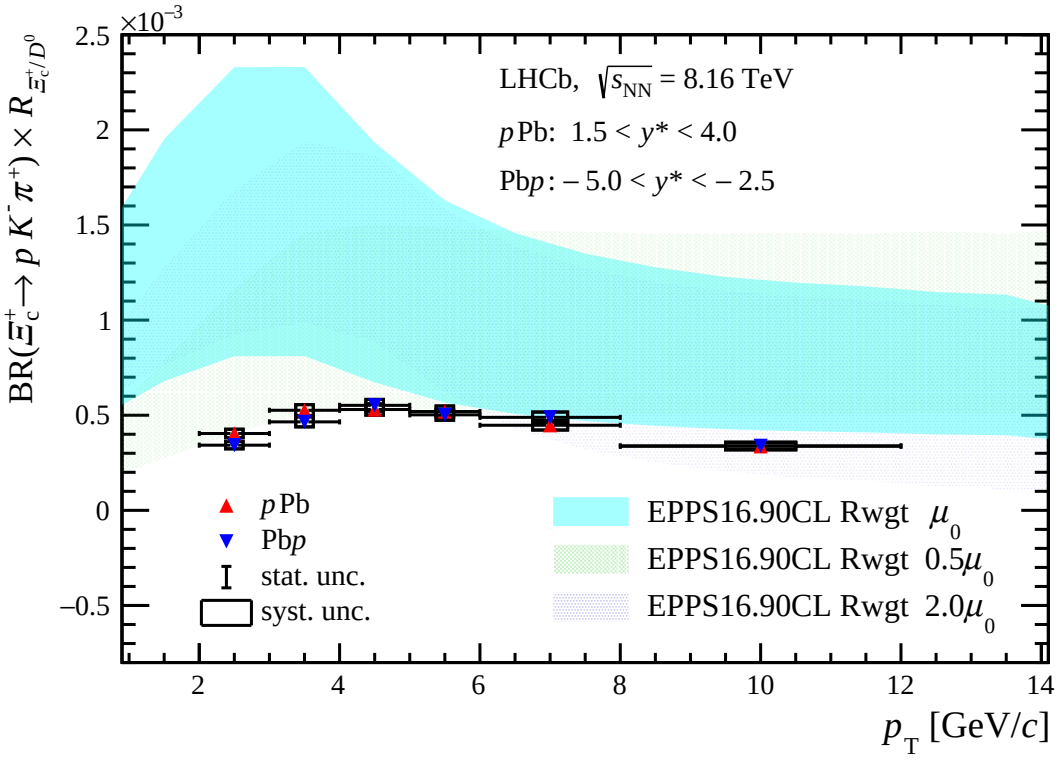


Figure 7: Production ratio of $\Xi_c^+$ to $D^0$ in $p$Pb (red triangles) and Pb$p$ (blue triangles) data samples as a function of $p_{\rm T}$. The error bars represent the statistical uncertainties while the squares denote the systematic uncertainty.